Inverted Pendulum Demonstration

Candidate Number: 8240R

Supervisor: Dr. Christopher Lester

The unstable point above a pendulum's centre of mass can be made stable by rapidly oscillating the support. This report will use this 'Dynamic Stability' condition to design and build an accurate and robust demonstration of the phenomenon, by using a jigsaw. Dynamic stability has important implications for any system that benefits from forced stability, from particle traps to high temperature superconductivity. The theory of dynamic stability is investigated and the state of research is summarised, with a review into previous designs used to justify our chosen design. A numerical integrator with an adaptive step is written and shown to accurately predict the pendulum dynamics. The frictional form of the pendulum is found to vary with the angular speed, by measuring the amplitude decay with a high speed camera. Subsequently, the exact frictional co-efficient of the pendulum is calculated and input into the model. Finally, the jigsaw is shown to exhibit inverted pendulum dynamics, and the minimum threshold frequency is measured for 5 different lengths. The data is revealed to be in good agreement with both the theoretical values and the computer model, and a relationship was found between the minimum frequency and the initial displacement.

1 Introduction

For over 300 years, Galileo's pendulum study has been one of the axioms of classical dynamics in mechanical systems.[1] However, a peculiar phenomenon occurs when the suspension point is vertically oscillated. The unstable point above the centre of gravity becomes dynamically stabilised, and can be shown to oscillate about this new stable position. Although extremely counter-intuitive, dynamic stabilisation is much more obvious in a gyroscopic-top or a man on a unicycle, both of which find stability by assuming the most vertical position.

Dynamic stability was first investigated by Stephenson in 1908, who found that stability can be incurred by periodic oscillations and applied to a pendulum with a rapidly vibrating support.[2] Kapitza further investigated the stability conditions and solved the arising Mathieu equation, before using successive approximations to solve the problem outside of the small angle approximation.[3] In addition, Kapitza experimentally investigated the conditions, building a 'Kapitza Pendulum', which used a rotary-to-linear device from a sewing machine to vertically drive a pendulum.[4] In 1985, Michaelis created an inexpensive demonstration of the phenomenon using a handheld jigsaw, and in 1992, the limits of the stability of the system were experimentally studied by fashioning an oscillator out of speaker-coils.[5–7] There have been numerous attempts at elaborating on the mathematics, by both considering sinusoidal oscillations, and non-parametric saw tooth oscillations which simplify the mathematics.[8–10] A large number of systems have equations of motion analogous to the Mathieu equation, and so can undergo dynamic stability. These include: particles in a cyclotron, levitating liquid droplets and confined charged particles in

a Paul trap.[11–13] Furthermore, there has been recent interest in the use of dynamic stability to create super-conducting states at room temperature.[14]

Although previous work has concentrated on the mathematics and stability conditions, here we will rigorously create a robust experimental demonstration of the inverted pendulum that gives accurate measurements, and can be used to display dynamic stabilisation to large audiences. Furthermore, a computer model will be created in tandem with the physical apparatus, and will be used to model the dynamics in the absence of mechanical vibrations or resonances.

The report will begin by summarising the theory of dynamic stabilisation, before numerically integrating the equation of motion in a computer model. Previous designs in the literature will be reviewed to help create our own inverted pendulum demonstration, and each feature will be justified. The friction of the pendulum will be determined, before the final model is used to compare the minimum frequency of oscillation with the theory.

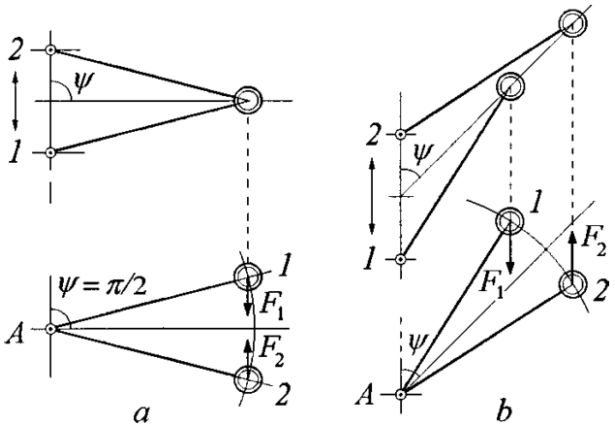

Figure 1: Force diagram of the pendulum perpendicular to the oscillations, and at an arbitrary angle ψ.[15]

2 Background Theory

2.1 Dynamic Stabilisation

Physically, we can understand dynamic stability by considering the torques acting. Neglecting gravity, if there is zero initial velocity and the rod is displaced perpendicular to the oscillations, in the inertial frame of the pivot the centre of masses (COM) are placed on a circular arc, as shown in figure 1a, with equal and opposite torques.

If the rod is at an arbitrary angle ψ above the horizontal, the forces are still the same, but the length of the moment is longer for position 2, as seen in figure 1b. If the angle was below the horizontal the converse would be true.

Thus, on average there is a greater restoring torque towards the upward vertical. In the presence of gravity, stability is achieved if this vibrational torque, averaged over many cycles, is greater than the gravitational torque.[15]

Consider a rigid pendulum of length l, mass m, and COM αl, with moment of inertia I_{COM}.

The pendulum's support is vertically displaced by a sinusoidal oscillation with driving frequency Ω and amplitude A: $a(t) = A\cos\Omega t$. At an angle θ from the upper vertical, the COM has x and y coordinates, $x = \alpha l\sin\theta$ and $y = \alpha l\cos\theta + a(t)$.

To derive the equation of motion we use Lagrangian mechanics.

As derived in the appendix(A.1), the Lagrangian in full is:

$$L = \frac{1}{2}m\big[(\alpha l\dot{\theta})^2 + \dot{a}^2 + 2\dot{a}\alpha l\dot{\theta}\sin\theta\big] + \frac{1}{2}I_{COM}\dot{\theta}^2 - mg(\alpha l\cos\theta + a(t)) \quad (1)$$

The Euler-Lagrange equation (2) can be used to derive the equation of motion:

$$\frac{d}{dt}\Big(\frac{\delta L}{\delta\dot{\theta}}\Big) - \frac{\delta L}{\delta\theta} = F_\theta \quad (2)$$

where the Dissipative Force F_θ will be elaborated upon in section 2.2.

Assuming $F_\theta = 0$, solving (2) using (1) yields the equation of motion:

$$\ddot{\theta} + \frac{\alpha}{\alpha^2 + \beta(\alpha)}\Big(\frac{\Omega^2 A}{l}\cos\Omega t - \frac{g}{l}\Big)\sin\theta = 0 \quad (3)$$

where $\beta(\alpha) = \frac{I_{COM}}{ml^2}$ as shown in A.1. This is a form of the Mathieu equation.

This motion is of similar form to a simple pendulum, with the acceleration due to gravity

modulated by a vertical driving force. As this form is analogous to a simple harmonic oscillator ($\ddot{\theta}+\omega^2\theta=0$), the period can be easily calculated from $T=2\pi/\omega$.

Ignoring friction, we can derive the condition for dynamic stabilisation by writing θ in terms of slowly varying variables: θ_1, C, and S:

$$\theta = \theta_1 + C\cos\Omega t + S\sin\Omega t \tag{4}$$

This allows us to write the equation of motion in terms of θ_1, assuming $\Omega^2 \gg \frac{g}{l}$, which is easily achievable with a powerful oscillator.

After some manipulation(see A.2), we find for small θ_1:

$$\ddot{\theta}_1+\frac{\alpha}{\alpha^2+\beta(\alpha)}\left(\frac{\Omega^2A^2\alpha}{2l^2(\alpha^2+\beta(\alpha))}-\frac{g}{l}\right)\theta_1=0 \tag{5}$$

The upright position is only stable if there is a restoring force in the direction of the upper vertical, thus the term in brackets must be positive.

The condition for stability is:

$$\Omega^2 > \frac{2(\alpha^2+\beta(\alpha))gl}{\alpha A^2} \tag{6}$$

This condition is important as it gives us the critical frequency, Ω_c, in which the constructed inverted pendulum will work; although we have neglected friction which may be important in the physical model. Later on, Ω_c will be investigated further, and used as a guideline for the parameters of our inverted pendulum.

2.2 Dissipative Friction

In any sort of physical system there will be frictional forces acting. The dissipative force is proportional to the velocity of the system, v, raised to some power n, and opposes motion:

$$F = -sign(v)^{n+1}\gamma v^n = -sign(\dot{\theta})^{n+1}\gamma(\alpha l\dot{\theta})^n \tag{7}$$

where γ is a constant, and the sign function ensures that the friction opposes motion.

If $n=0$, the friction is directly proportional to the contact force and independent of speed or area, and is known as dry friction. Viscous friction, given by $n=1$, increases linearly with v. High velocity friction, $n=2$, tends to dominate when the speed v is very large, or in high Reynolds number regimes.[16]

In an ideal pendulum system, the friction term is proportional to $\dot{\theta}$, however care will be taken in this investigation to measure n.[17] The final dissipation function[18] is derived in A.3, and F_θ is found to be:

$$F_\theta = -sign(\dot{\theta})^{n+1}\gamma(\dot{\theta})^n \tag{8}$$

In section 5, the friction will be investigated to find n.

3 Computational Method

3.1 Adaptive Step Runge-Kutta Method

Although (3) can be solved analytically using the Mathieu equation, here the Runge-Kutta (RK) method with an adaptive step will be used to integrate the differential equations numerically.[19]

The RK method performs a number of steps at different points along the interval and finds a weighted average, which is dependent upon how close the steps are to the midpoint.[20]

We will use the adaptive step Runge-Kutta-Fehlberg method, which removes the step size dependence by including a procedure to see if the proper step-size, h, is being used.[21] If we perform a step h_1 with error e_1, the optimal step-size h_2 that gives an error equal to the tolerance ϵ is:

$$h_2 = 0.9h_1\left(\frac{e(h_1)}{\epsilon}\right)^{\frac{1}{5}} \tag{9}$$

The extra 0.9 is added as a small margin of safety for any approximations made. If $h_2 \geq h_1$, then h_1 is accepted, otherwise the integration is repeated with h_2 (for full consideration see A.4).

The parameters inputted into the model are the maximum tolerance and maximum time. The algorithm proceeds step by step until this tolerance is exceeded or the maximum time is reached.

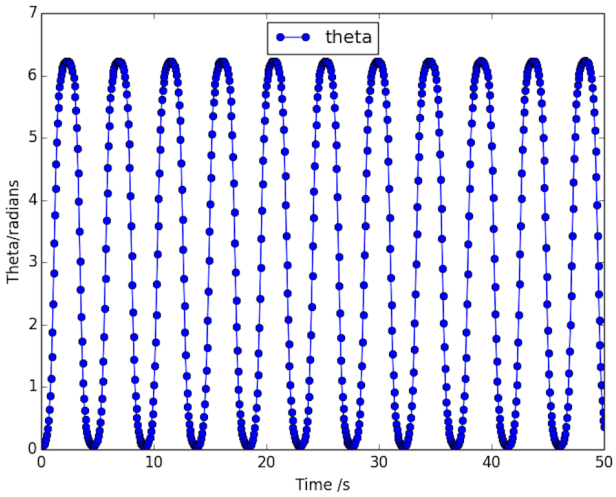

Figure 2: Computational model of θ vs t for an ideal pendulum, starting at $\theta_0 = 0.005^c$.

3.2 Testing the Model

The equation of motion for a simple pendulum was inputted into the algorithm as two coupled first-order differential equations:

$$\dot{\mathbf{y}} = \begin{bmatrix} \dot{y_0} \\ \dot{y_1} \end{bmatrix} = \begin{bmatrix} y_1 \\ f(\alpha)\left(\frac{g}{l} - A\Omega^2 \cos \Omega t\right) \sin y_0 - F_\theta \end{bmatrix} \tag{10}$$

with initial conditions:

$$\mathbf{y}(0) = \begin{bmatrix} \theta_0 \\ 0 \end{bmatrix} \tag{11}$$

where θ_0 is a small displacement from the upper vertical, and $f(\alpha) = \frac{\alpha}{\alpha^2 + \beta(\alpha)}$.

The algorithm was run for 50 seconds with $h = 0.005s$, $\theta_0 = 0.005^c$, and $\epsilon = 10^{-9}$. θ against time is plotted in figure 2, and the x and y positions of the rod are plotted in figure 3.

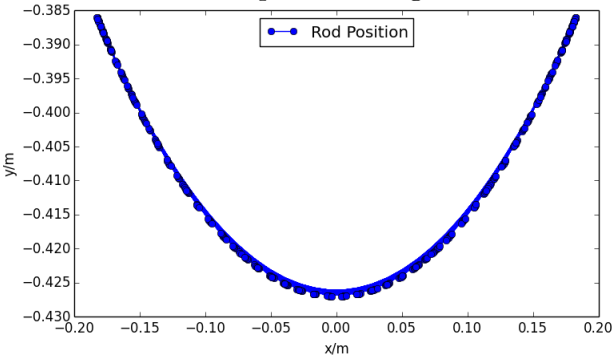

Figure 3: Trace of pendulum rod length $l = 427mm$ in xy plane. The bottom half of the motion is shown.

3.2.1 Adaptive Step

Next the adaptive step-size was checked. The step-size should adapt and change depending on how rapidly the underlying function varies.

To test this hypothesis, a simplified version of equation (3) was numerically integrated:

$$\ddot{\theta} - \frac{\alpha}{2\alpha^2 - \alpha + \frac{1}{3}} \frac{g}{l} \sin\theta = 0 \tag{12}$$

The step-size h is plotted in figure 4.

Comparing figures 2 and 4, we can see the step-size pattern matches the sinusoidal behaviour. As expected for the more linear regions at $\theta \pm \pi$, h has a larger step size of around $0.1s$, but as the curvature increases nearer the $\theta = \pm 2\pi$, a smaller step-size of $0.05s$ is required.

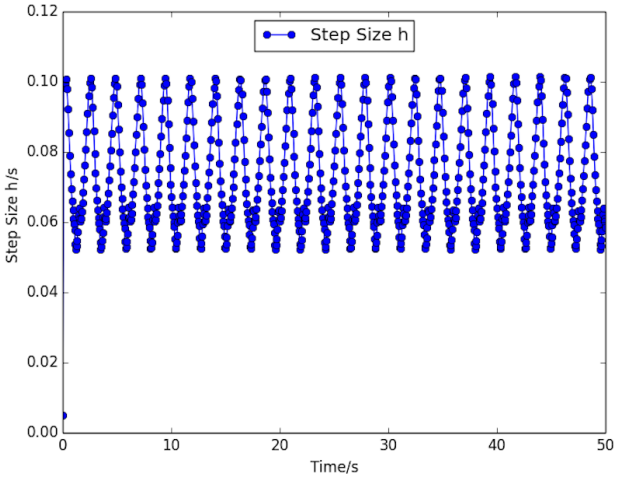

Figure 4: Plot of step-size h vs Time in seconds. There is a clear pattern matching the sinusoidal behaviour.

3.2.2 Conservation of Energy

With no external forces acting, the integrator should conserve energy. The total energy was calculated at each step for 10000 steps, with $\epsilon = 10^{-9}$, and subtracted from the initial energy.

Figure 5 illustrates that increasing the step number causes the error in the energy to accumulate, increasing the energy difference. However, as the total energy is of order $10^{-1}J$, and the total accumulation is of order $10^{-10}J$, this accuracy is adequate for a large number of steps.

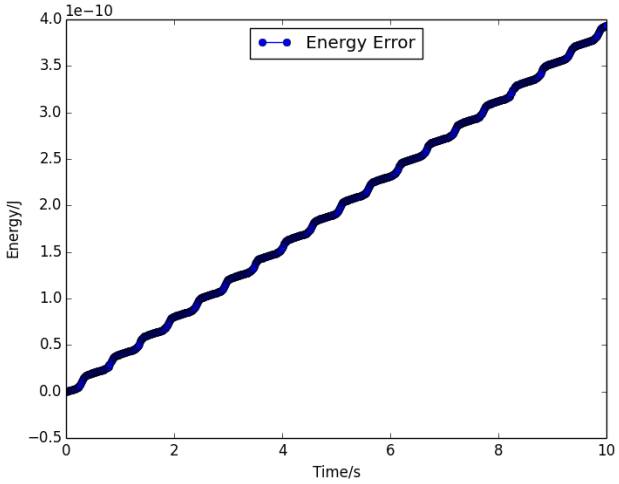

Figure 5: The total energy difference starts to deviate from 0 as the number of steps increases.

3.2.3 Analytic Comparison

The difference between the simulation and the analytic solution of a simple pendulum was calculated, to test the accuracy of the integrator. By solving (3) using the small angle approximation $\sin\theta \approx \theta$, we find that:

$$\theta(t) = (\pi - \theta_0)\cos\sqrt{\frac{\alpha g}{(2\alpha^2 - \alpha + \frac{1}{3})l}}t \qquad (13)$$

Figure 6 shows the normalised difference. As the analytical solution is only valid for small angles, there is greater error at the maximum amplitudes, which accumulates to $3\text{x}10^{-4}$ over $55s$.

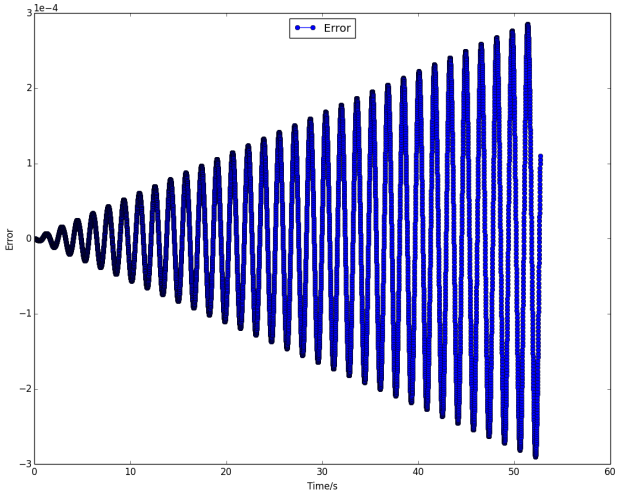

Figure 6: Plot showing normalised error between computed dynamics compared to analytic solution for $\theta = 0.1^c$. At the max θ the error accumulates.

4 Pendulum Design and Construction

4.1 Previous Designs in the Literature

The major goal of this project was to build a robust demonstration of an inverted pendulum. The most important characteristic of the design is the ability to oscillate above Ω_c. There are a number of examples of inverted pendulums in the literature, and care was taken to investigate which design would be most suitable for this project.

4.1.1 Flywheel Driven Pendulum

In 1954, Kapitza used a rotary-to-linear mechanism from a sewing machine to create an inverted pendulum, shown schematically in figure 7.[14]

As figure 7 (inset) illustrates, the amplitude is of the same order as the radius (assuming $\frac{L}{L'} \approx 2$). Hence, this design could have a large amplitude and so a small Ω_c. For $l = 0.2m$, and $A, r = 0.1m$, we find that $\Omega_c \approx 14 rads^{-1}$ or $2.22 revs^{-1}$, roughly equivalent to a slowly moving bicycle wheel. However this method was not chosen as the set-up is too bulky and there may be issues if A is of similar length to l.

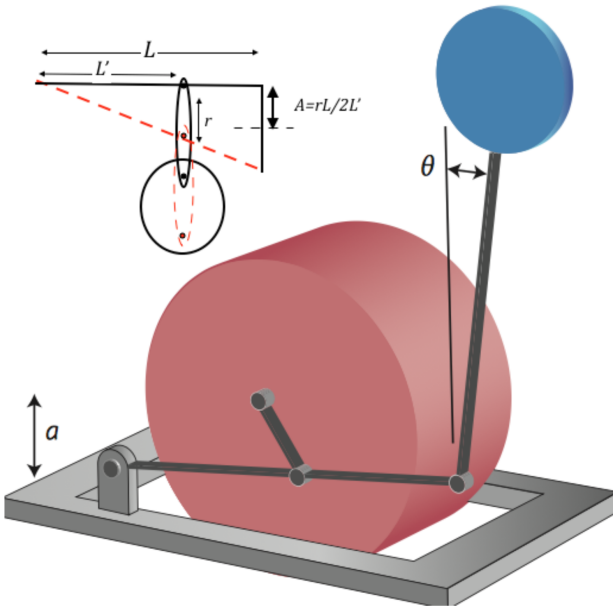

Figure 7: Possible flywheel pendulum design, with geometric proof of amplitude inset.[14]

4.1.2 Speaker Cone Driven Pendulum

An exposed speaker cone vibrates vertically at high frequencies. By controlling the voltage across the speaker cone, Smith and Blackburn, among others, were able to accurately control the oscillation frequency and measure the stability of the system. The set up they used is shown in figure 8.[22]

However, oscillations will only work for very small pendulums of $l \approx 0.01m$ as the amplitude is very small, thus it becomes difficult to measure the frequency or use for a demonstration.

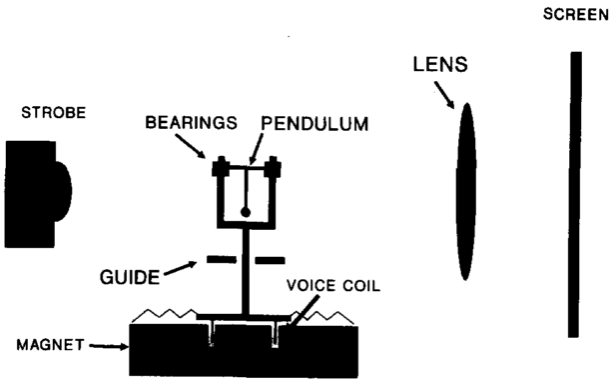

Figure 8: Set up using speaker cone as driver. Includes apparatus for measuring frequency.

4.1.3 Jigsaw Driven Pendulum

A jigsaw can be used to achieve dynamic stabilisation by attaching a pendulum rod to its rapidly oscillating saw piece. Although arguably the most crude configuration, this set-up, as illustrated in figure 9, has proved surprisingly useful.[23] Numerous groups have been able to fashion a pendulum to the fragile saw-blade and witness the phenomenon, as the saw can oscillate at high frequencies.[5,6] However, there are a number of caveats to the design:

- Jigsaws tend to have small amplitudes, of around 10mm, which requires a powerful saw with high Ω.
- Modern jigsaws tend to have a pendulum function built-in which rocks the blade.
- The blade can be very fragile and therefore unsuitable to be used as an oscillator.
- Many jigsaws only have a limited range of speeds, and so it may prove difficult to perform any meaningful analysis.

However, the robustness of the build, and the ability to have a powerful, semi-portable oscillator, made the jigsaw the most appealing choice, and care was taken to overcome the issues listed above.

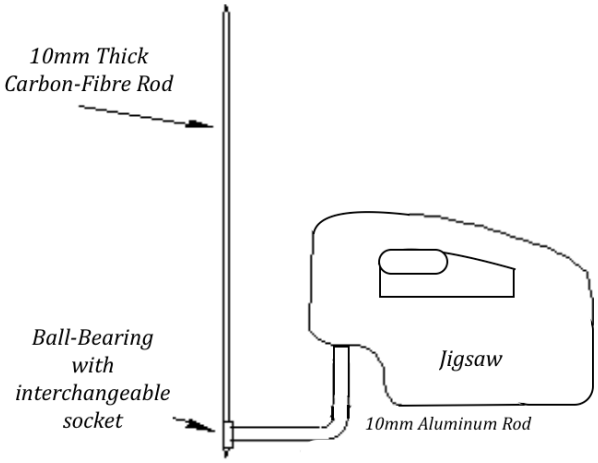

Figure 9: Schematic of chosen design. Jigsaw arm connected to ball bearing joint with interchangeable pendulum rods.[23]

4.2 Design of the Jigsaw Pendulum

The Wickes PSJ800X jigsaw was chosen as the base.[24] With a large number of speeds and the ability to turn off the pendulum motion, the jigsaw fulfilled the required criteria, whilst costing a fraction of the price of similar models.

To overcome the problem of the fragile blade, the pendulum's support was fashioned to an arm that connects directly to the saw's internal mechanism. Notwithstanding, this caused a slight deflection at the end of the arm, whilst the extra mass put more pressure on the saw's mechanism. Thus, the arm was machined to be as short as possible.

A ball-bearing joint was connected to the end of the arm, allowing 2π radians of theoretically frictionless planar movement. Furthermore, the joint's screw-hole allowed different lengths of rod to be attached. This added another controlled variable and negated the issue of less variation

in the oscillating speeds, compared to other designs.

The Wickes jigsaw has an amplitude A of $10mm$, which required a frequency of around $120rads^{-1}$ for the pendulum's length of $O(100mm)$.[24] This is a relatively high frequency, and so a balance between the robust materials used and the mass of the system was needed.

Both the pendulum's arm and rods experienced a deflection as shown in figure 10:

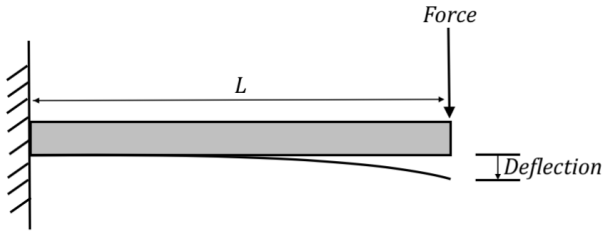

Figure 10: Schematic diagram showing cantilever beam deflection.

The deflection experienced by the rod can be modelled using the Euler-Bernoulli beam bending equation and is dependent upon the force acting F, the Young's modulus E and the moment of inertia of the beam I:

$$\delta = \frac{Fl^3}{EI} \tag{14}$$

Care was taken to minimise deflection by choosing materials with large E and I, and minimising l if possible, as too much flex would cause the pendulum rod to become unstable and fall.[25]

The pendulum arm was chosen to be made from aluminium, a light metal, with a high E of $69GPa$.[26] The arm itself was a hollow $10mm$ thick tube which was lighter and had a higher I per unit mass than a rigid rod.[27]

There were a number of options for the shape of the rod: I beam, solid rod or hollow rod/tube. This list was narrowed down to the solid and hollow rods, as the I beam was neglected due to mechanical difficulties in creating the shape.

The moment of inertia of a uniform cylinder about one end can be derived by similar means as shown in A.1, and it is found that:

$$I = \frac{M(r^2 + r_i^2)}{4} + \frac{ML^2}{3} \tag{15}$$

where r_i is the inner radius of the hollow cylinder.[27]

If the cylinder is very long, $L >> r$, and the hollow and solid rods have an identical radius, r, they will have the same I. Thus, the solid rod was chosen as it was heavier and had a higher overall I.

The rods were made from carbon fibre which offered the best stiffness to mass ratio, as shown in the Ashby Property map in figure 11, and were not too expensive to buy or machine.[28,29]

5 pendulum rods of lengths $0.1m - 0.5m$ were machined, giving a range of Ω from $100rads^{-1} - 300rads^{-1}$ which was within the capabilities of the jigsaw.

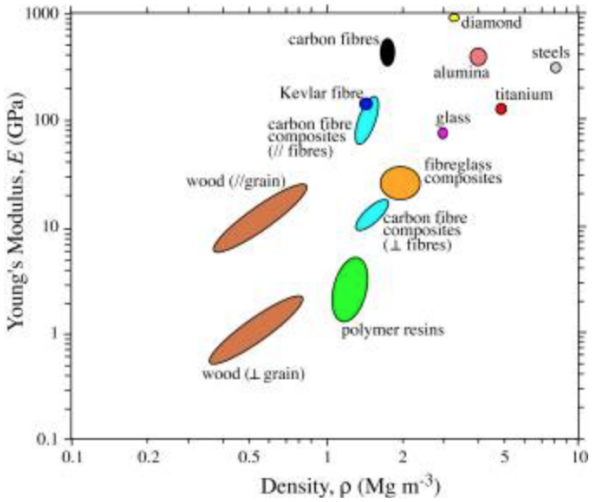

Figure 11: Ashby Property map.[28] Graph shows Young's modulus E vs density for different materials.

4.3 Construction of The Pendulum

The jigsaw created very fast oscillations by having a small internal flywheel, rotating at high speeds, directly driving the saw.

An aluminium rod was shaped into a right angle bend and the arm was welded directly to the inner mechanism.

The main source of friction arose in the bearing's metal shield, which increased friction but prevented dust building up. There were more expensive, smoother ceramic bearings but a noticeably better ceramic bearing was outside of this project's budget.

The end of the arm was tapered and the inner ring of the ball bearing was attached to the ta-

pered end, with care taken to preserve the workings of the bearing. A connector with a screw-hole was connected to the outer ring of the bearing, allowing for interchangeable rods. The labelled apparatus is pictured in figure 12.

Mass g	Length mm	α
28±0.1	127±1	0.32±0.03
39±0.1	227±1	0.33±0.02
51±0.1	327±1	0.35±0.01
61±0.1	427±1	0.36±0.01
72±0.1	527±1	0.40±0.01

The length of each rod, including the connector, is given in the above table. The errors arose due to the limitations of the measuring equipment; a ruler and weighing scales.

The COM of the rod was no longer in the centre, so α was measured by balancing each rod on a narrow pivot and marking the position in which the rod was balanced. There was a larger error in the COM measurement of $\pm 4mm$.

Throughout this report, the errors were calculated using a Taylor expansion formula, which is explained in detail in A.5.

The overall error in α, σ_α, was calculated by expanding the function $\alpha = \frac{L_{COM}}{L}$:

$$\sigma_\alpha^2 = \left(\frac{\partial \alpha}{\partial L}\right)^2 \sigma_L^2 + \left(\frac{\partial \alpha}{\partial L_{COM}}\right)^2 \sigma_{L_{COM}}^2 \qquad (16)$$

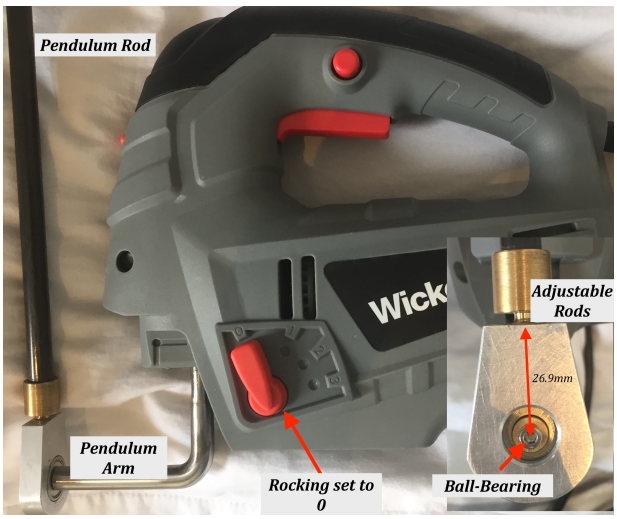

Figure 12: Labelled image of final jigsaw set-up. Inset is a magnified image of the connection.

5 Measuring Friction

Before the computational model can be used to predict the dynamics, the form of the friction entering into the Lagrangian must be determined. In this section, the friction will be measured by recording the pendulum's movement and analysing the results.

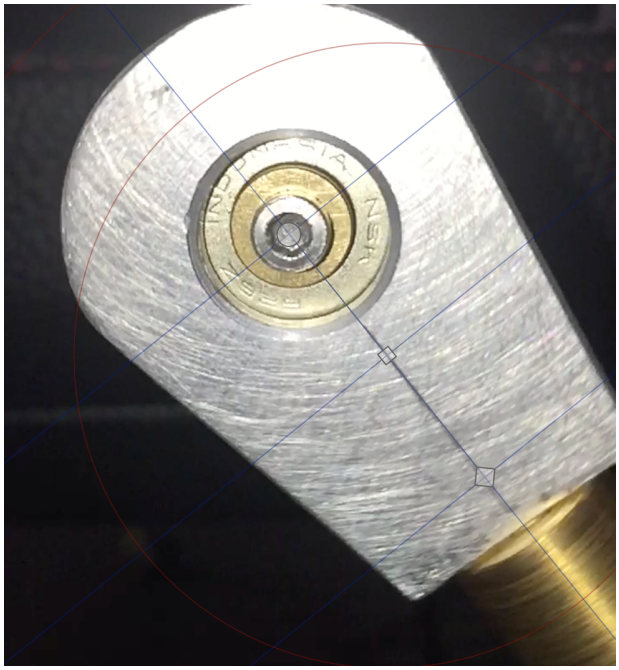

Figure 13: Image of the clamped support, with the protractor software overlaid.

5.1 Method

The pendulum's motion was recorded using a high definition slow motion camera recording at $240fps$ and the angle was measured using on-screen protractor software.[30]

The jigsaw was clamped and well-lit, as shown in figure 13.

To eliminate parallax error, the camera was placed as close as possible to the pivot. Furthermore, to assist in taking measurements, a straight line was drawn on to the front of the pivot.

The angle, $\phi(t)$, was measured from the downward vertical, $\phi(t) = \pi - \theta(t)$.

The protractor software allowed very precise measurements to be taken to $\phi = \pm 0.001°$. However, we were only able to achieve an accuracy

of $\pm 1^\circ$ due to the finite resolution of the video.

The software also measured the angle from an arbitrary vertical on-screen. Thus the readings were adjusted using the 'zero-point' value of ϕ, which is the value of ϕ on-screen when the pendulum was actually at $\phi = 0^\circ$.

Although the accuracy of the video is 240fps, there was some sampling error, as it was difficult to judge the point of maximum amplitude. To help our observations, the time was also adjusted so $t_0 = 0s$,which gave an overall error in the time of $\pm 0.05s$.

To determine the value of n, the maximum amplitude was recorded for each half-period and compared to a range of different frictional terms in the model.

5.2 Results and Discussion

5.2.1 Determining n

The motion of the pendulum was recorded, and the maximum angle from the downward vertical, $\phi(t) = \pi - \theta(t)$ is plotted in figure 14.

There is clearly a decay of amplitude, as the pendulum loses energy due to friction, and the decay time increases with pendulum rod length.

There were issues with recording the final few oscillations, which stopped much faster than expected, making it hard to differentiate between the final amplitude and the resting position.

This was best observed for $l = 127mm$, which had an equilibrium position after oscillation 1° above the equilibrium $\theta = 0^\circ$.

As explained later, there may have been issues with the bearing causing different frictional regimes at different values of θ.

To determine n, the oscillating frequency was turned off in our model, and the initial amplitude was set to $\theta_0 = 2.8^c$.

Friction of the form θ or $\ddot{\theta}$ causes only a shift in the period of oscillations, therefore only $\dot{\theta}$ will be investigated. The error in ϕ was calculated to be $\pm 1.4^\circ$, which includes the zero-point error.

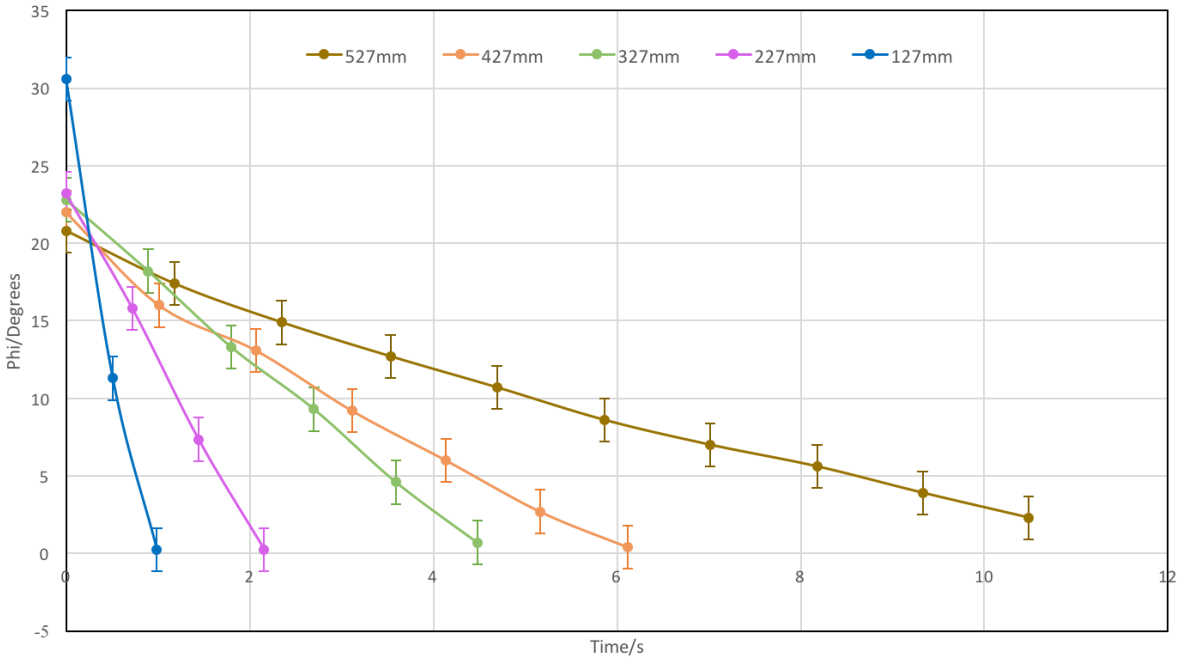

Figure 14: Plot of amplitude decay for 5 different lengths of rod. As the length increases the pendulum's lifetime increases. Error bars of $\phi = \pm 1.4^\circ$ are shown. Error in $t = \pm 0.05s$.

5.2.2 $n = 2$

First consider a $n = 2$ friction term. The *sign* function ensures the friction opposes the motion.

Figure 15 shows the simulated model with low and high friction, compared to the data.

In the lower friction regime, the simulation matches the data initially. However, the data decays more rapidly than the simulation, which has a longer tail of smaller oscillations due to the $\dot{\theta}^2$ term. For higher friction, the initial amplitudes do not fit the data and the characteristic longer tail of small oscillations for $t > 10s$ is still present.

The $n = 0$ term is also shown not to fit the data in $A.6$, as it predicts a very linear decay.

5.2.3 $n = 1$

For an ideal pendulum ($\ddot{\theta} + 2\gamma\dot{\theta} + \omega^2\theta = 0$), the motion has an analytical solution:

$$\theta(t) = \theta_0 e^{-\gamma t} \cos \omega t \tag{17}$$

assuming $\gamma \ll \omega$.

At the maximum amplitude the cos term is 1, so we can rearrange (17) to find a straight line equation with gradient $m = -\gamma$:

$$ln\left(\frac{\theta max}{\theta_0}\right) = -\gamma t \tag{18}$$

The amplitude ratios for the different lengths are shown in figure 16 overleaf. The decay of each rod seems to show a similar pattern, with a flatter γ at larger amplitudes, and steeper γ at smaller amplitudes.

In A.5, it is shown that the error in the logarithmic term is inversely proportional to the ratio between the initial displacement and the displacement per period. Hence, our values near the end of the cycle have much larger errors than the initial readings.

5.2.4 Determining γ

The data does not fit the simple model (18), with the gradient of all the lines increasing for smaller ϕ.

Figure 14 is in agreement with this, with all of the decays having a much flatter middle region than a simple exponential decay. This indicates two decays occurring; one with a longer lifetime than the other, giving a flatter curve.

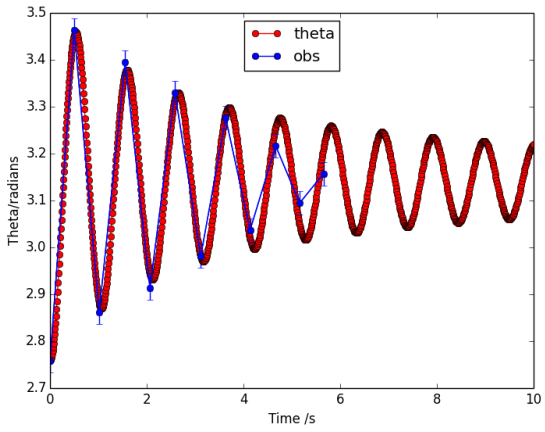

(a) n=2 with low friction

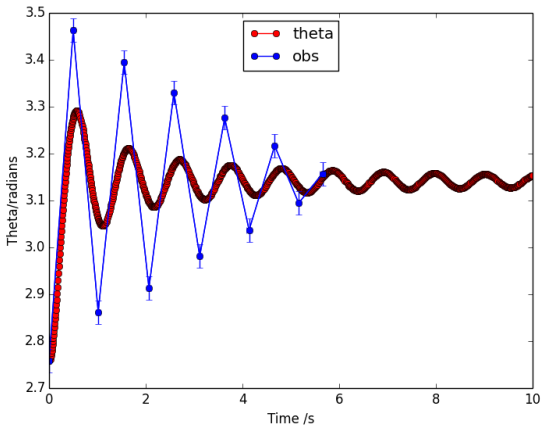

(b) n=2 with high friction

Figure 15: Lower friction n=2 matches the data initially. However, the data decays more rapidly than the simulation which has a much longer lifetime. For higher friction there is a longer lifetime but we still see the small oscillations for $t > 10s$ unlike the data. Error bars are $\pm 0.025^c$

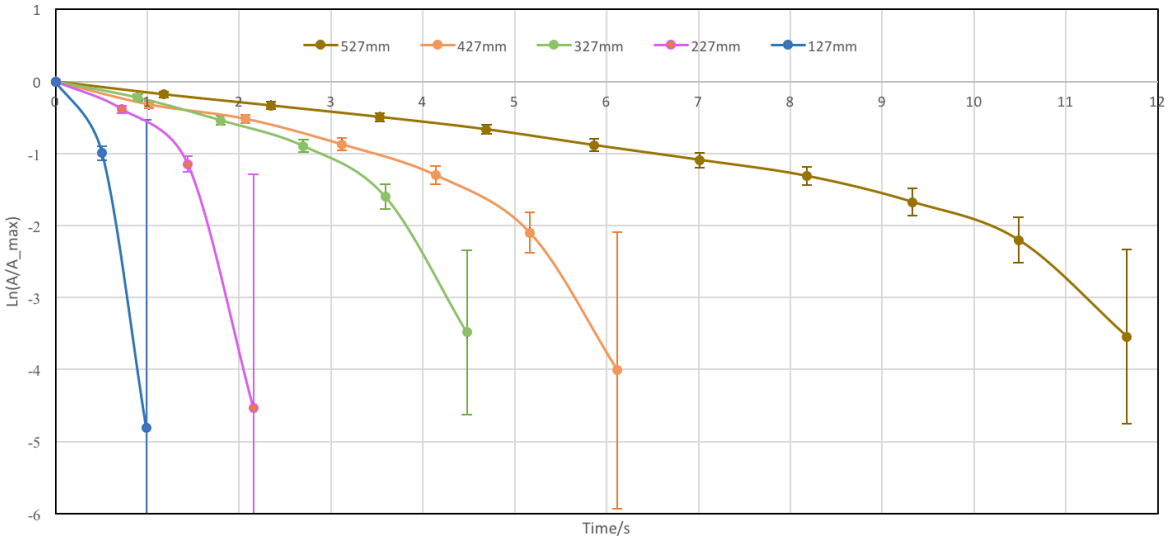

Figure 16: Plot of natural log of the amplitude ratio vs time. The error in the ln term is inversely proportional to max angle per cycle, so increases at later cycles. As expected the longer rods have lower gradients and thus smaller γs.

The gradient of each line was measured using a linear regression model. Looking at the data in figure 14, there are two clear regions of differing γ, $5° \leq \phi \leq 20°$ and $0° \leq \phi \leq 5°$. For $l = 527mm$, the linear regression, shown in figure 17, exhibits a good fit. However, as there is only 3 measurements used to find the gradient for the latter region, the linear regression is not precise, especially as there is such a large error on the final reading.

The linear regression was performed for each length and the results are summarised in the table above. Each regression is shown in $A.8$.

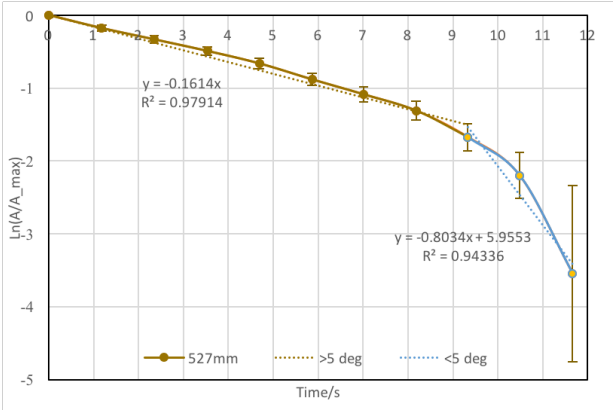

Figure 17: Detailed plot of logarithmic behaviour for $L = 527mm$. Linear regression was performed for $5° \leq \phi \leq 20°$ and $0° \leq \phi \leq 5°$.

Length m	γ for $\phi < 5°$	γ for $\phi > 5°$
127±1mm	7.95	1.96
227±1mm	4.74	0.78±0.15
327±1mm	1.45±0.38	0.33±0.02
427±1mm	1.36±0.35	0.30±0.02
527±1mm	0.8±0.2	0.17±0.01

The errors above are only due to the error of the fit and do not consider the error in the data. There are no errors for $l = 127mm, 227mm (\phi < 5°)$ as there are not enough values to work out the error of the straight line.

This is a good assumption for the $\phi > 5°$ regime, as the percentage errors are $< 10\%$, and the linear fit is within the error bars.

However, for $\phi < 5°$, there is a massive percentage error $> 80\%$, giving a much larger error in the gradient.

There are a number of reasons for lack of fit. The apparatus is relatively crude and there was horizontal movement of the apparatus' arm for $\phi \geq 10°$. Although this was minimised by resetting the protractor to a different origin point before each measurement. Furthermore, the ball-bearing movement may have been less smooth and so had a larger γ at slower speed or lower amplitudes. This would explain the tendency for the shorter rods to come to rest at an angle to the equilibrium position.

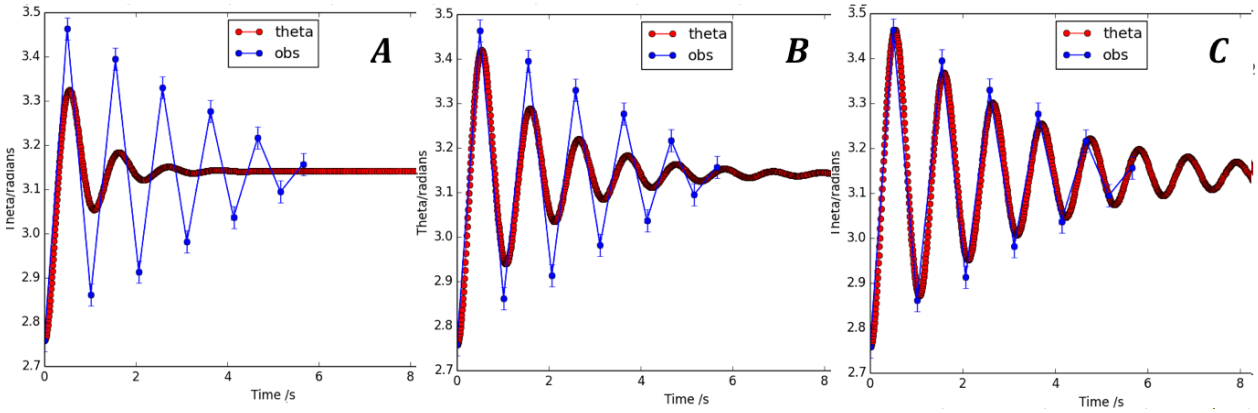

Figure 18: Comparison of observed behaviour of $l = 427mm$ with computed dynamics for different γ. Error bars are $\pm 0.025^c$. A: $\gamma = 1.36$. Poor match for number of decays and amplitude size. B: $\gamma = 0.6$. Good match for number of decays, but after initial decay the amplitude of the computed dynamics is much less than the observed. C: $\gamma = 0.3$. Good match of size of amplitude but underestimates lifetime with many more decays than the observed data.

γ can be found by fitting the model to the data, either by considering the number of oscillations, or the size of the amplitude per oscillation.

The different options are summarised in figure 18, which shows that the behaviour of $l = 427mm$ depends heavily on γ.

In A, $\gamma = 1.36$ is clearly a poor fit to the data, as the data decays many more times than the computed model, and the amplitudes do not match.

In B, $\gamma = 0.6$. There is a good fit with number of decays but the amplitudes do not match.

In C, we used the γ derived above in the linear regression($\gamma = 0.3$). By definition the model matches the data's amplitude well but the motion of the observed data abruptly stops after 6 oscillations.

This process was carried out for each length and the γ, derived from $\phi > 5°$, gave the best match of amplitude decay, as expected.

The biggest issue we faced when measuring the minimum amplitude was that large deviations from $\phi = 0°$ caused the system to become unstable and fall, so accurately modelling the amplitude decay was vital.

Moreover, the final sharp decrease in amplitude was probably due to an issue with the ball-bearing rubbing up against its casing or against the arm, causing a frictional build-up at low amplitudes when there is little energy in the system.

For these reasons, it was decided that the amplitude matching γ, from the $\phi > 5°$ region, provides the best description of the dynamics, within the bounds of this project.

6 Measuring Minimum Frequency

6.1 Method

A slow motion camera was used to record the motion of the pendulum, and the period was calculated by counting the number of frames required for one full oscillation. As a safety precaution, health and safety guidelines were adhered to by only operating the jigsaw for a maximum of 15 minutes daily.[31]

There was a sampling error of $\pm 2 frames$ or $\pm 0.01s$ per reading, which was minimised by recording 100 oscillations.

Ω_c was then calculated, using the simple rules described in A.5, to an accuracy of $\pm 0.3\%$.

For the computer model, the previously measured data was inputted, using the $\phi > 5°$ γs that fitted the amplitude decay, as mentioned earlier.

This decision was justified, as the physical pendulum had a tendency to drift out to higher

amplitudes. The model had an initial displacement of $\theta = 5°$ and the tolerance was decreased to 10^{-6} due to the adaptive step accumulating error, as shown in figure 19 and explained in A.7.

From the operating manual of the pendulum, the size of the oscillation is half of the stroke length or $10mm \pm 0.5mm$.[24] This error had to be assumed due to the lack of information from the company. However, it was decided that a 5% error seemed reasonable for a production line tool.

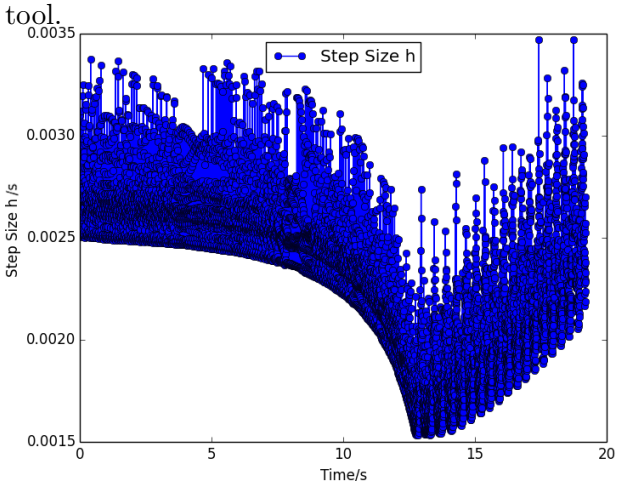

Figure 19: Plot of the behaviour of the adaptive step just below the threshold Ω_c. The behaviour closely matches the θ behaviour below the critical condition, with a decrease in h due to an increase in θ.

6.2 Results and Discussion

6.2.1 Computer Model

The simulation was run near the theoretical frequency, and the smallest value that caused the unstable point to become stable was recorded. Figure 20 is a plot of the behaviour near the minimum frequency at $\Omega = 205.06 rads^{-1}$ and $\Omega = 205.07 rads^{-1}$ for $l = 327mm$.

Below the threshold, there was initially no θ movement until the rod started to fall after 10 seconds. In contrast to this, just above the threshold, the rod slowly moved toward $\theta = 0$, and there were no oscillations due to the heavy damping and small initial displacement.

This behaviour can be explained as the forces are balanced and so the rod does not move. However, slightly above and below the threshold there is a slightly larger force and so after some time, the rod accelerates.

As we expect no movement at the critical frequency, the frequency difference between just above and just below the threshold gives us the error in Ω_c of $\pm 0.01 rads^{-1}$.

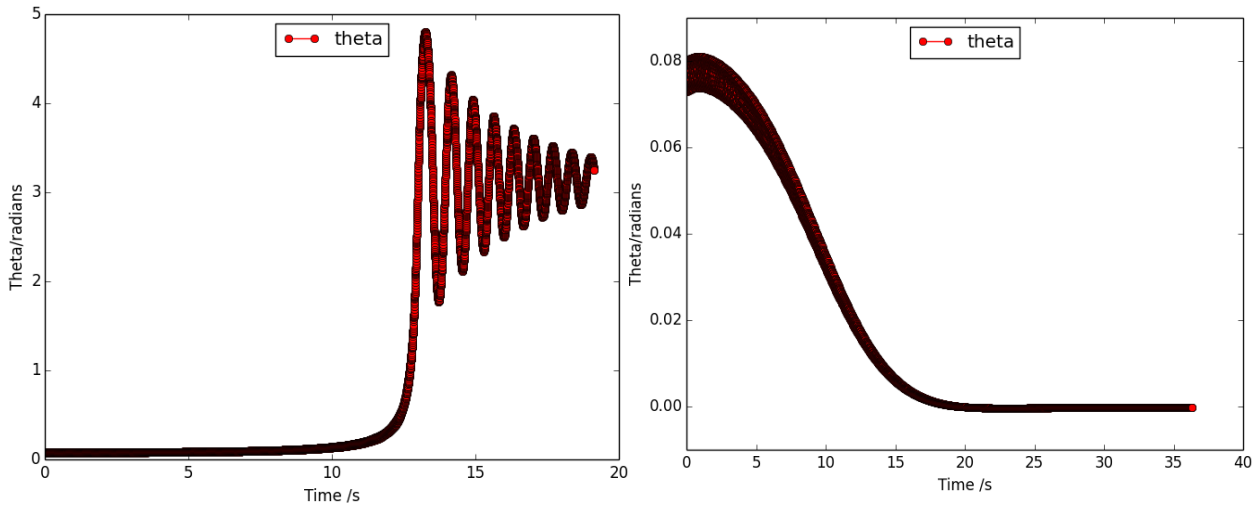

(a) Ω below threshold

(b) Ω above threshold

Figure 20: Just below the threshold, the pendulum stays at its maximum for over 10 seconds before falling toward the lower point. Above the threshold, the behaviour is similar except for a slow oscillation back to $\theta = 0$ with little oscillations due to friction.

Figure 21 shows an increase in Ω_c with initial displacement θ. At small angles, changing θ has little effect on Ω_c but there is an increase when $\theta \geq 15°$. This also explains figure 20, as a slight increase in angle increases Ω_c, and causes a snow ball effect. Thus the pendulum falls.

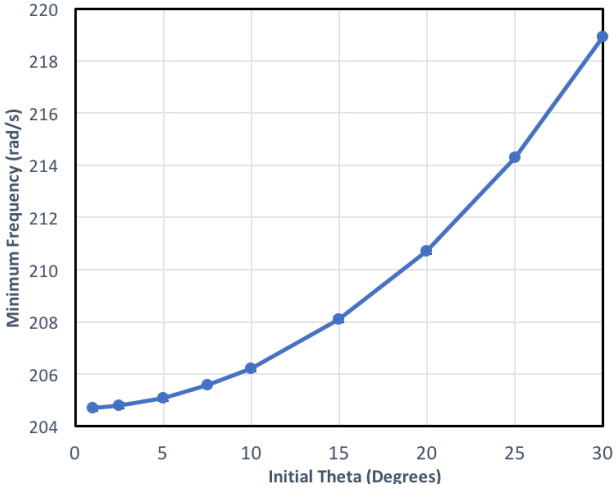

Figure 21: Plot of minimum frequency vs θ. Increasing the initial angle requires a higher frequency to achieve stability. The error in the frequency is $\pm 0.1 rads^{-1}$.

Friction had little effect on the minimum frequency. Changing the friction by 3 orders of magnitude caused the frequency to change by about $0.5 rads^{-1}$ but this project did not have time to investigate this limitation fully.

6.2.2 Theoretical Condition

Equation (6) was used to calculate the minimum theoretical Ω_c. To find the error in the theoretical value, the Taylor formula was used as shown in $A.5$.

The dominant source of error is in the amplitude A. As the other errors are negligible, the % error in Ω is equal to % error in A, which we have assumed to be 5%.

6.2.3 Comparison

The previous results were then compared to the observed data as shown in figure 22.

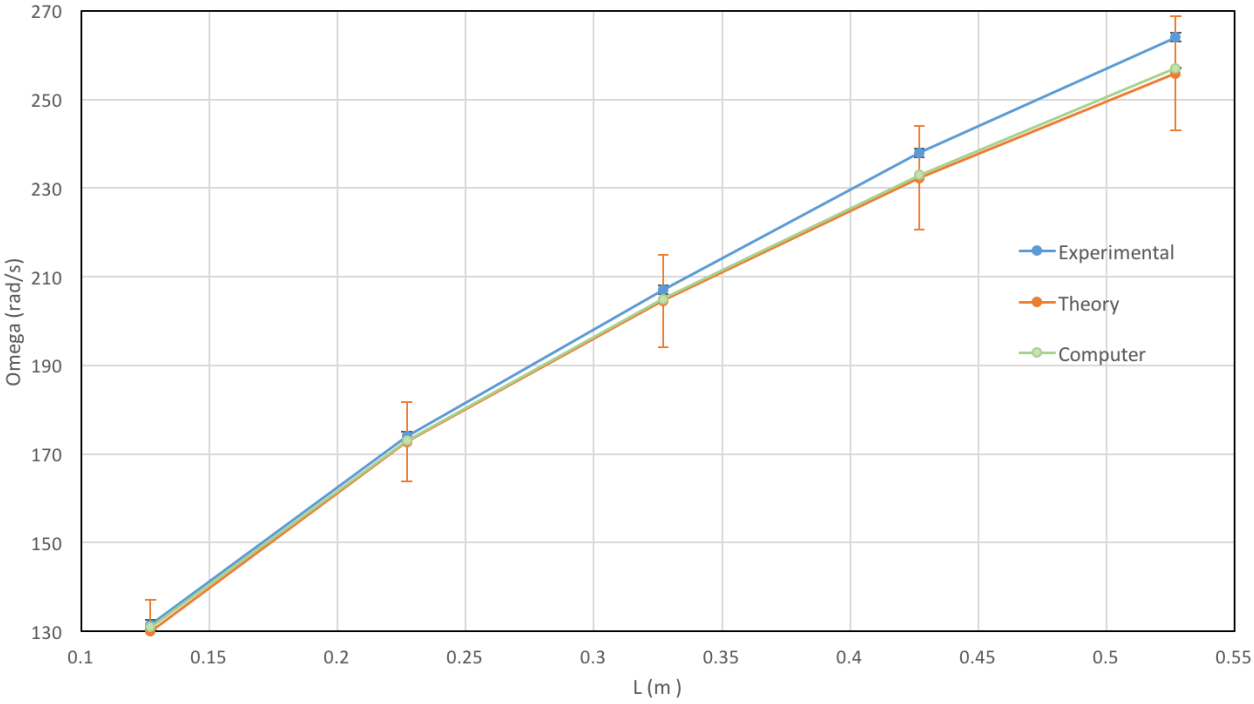

Figure 22: Plot of the minimum frequency Ω_c vs length l. The results are in good agreement with one another, with the model and the measured data closely matching the theoretical prediction. There is a deviation observed at larger l in the measured data due to the rod wobbling at higher frequencies. The error in the theory is 5%, the error in the simulation is $0.01 rads^{-1}$, and the error in the measured data is about 0.3%.

It is clear from the data that our inverted pendulum demonstration is accurate, as the data agrees with the theoretical model within the error bars. However, there is a systematic deviation at longer lengths due to greater vibrations at higher frequencies. The longer rods wobbled and regularly fell out of stability as θ increased, so higher frequencies were needed to reach the stability condition. The computer model is slightly higher than the theory, which is due to the fact that the theory assumes a tiny deflection, whereas in the model we displaced the rod by $\theta \approx 5°$, and the small angular increase gives a small increase in Ω_c as shown earlier.

The error in the theoretical results is large, and is due to the assumed error in the stroke length. However, this project did not have the time to further investigate a method to measure the stroke length accurately.

7 Conclusion

This project set out 3 main objectives: to build a robust working demonstration of an inverted pendulum, to write an algorithm that can be used to test the limits of dynamic stability, and to experimentally measure the friction and the minimum frequency condition.

The results in section 6 have shown that the demonstration is accurate, with the observed data matching the model within error. The apparatus proved to be robust, and will make for an inspiring and thought-provoking demonstration for those familiar with the simple pendulum. However, more work could be done in eliminating the friction and mechanical noise in the apparatus, by acquiring a more expensive bearing. Also, as the deflection is proportional to l^3, a small decrease in the pendulum arm should greatly decrease the deflection. The dominant source of error was due to the error in the stroke length, and with time this could be easily measured to increase the accuracy. The friction was measured and shown to fit the data. However as features from $n = 0$ and $n = 2$ were observed in the data, one could record the motion using a particle tracking system and calculate the exact value of n.

The computer model was shown to be an accurate simulation with a working adaptive step. The model was a useful tool as it allowed us to focus on the physical system in the absence of mechanical vibrations. The simulation also allowed an investigation into the limitations of the stability condition, and it was shown that the size of the deflection increased Ω_c, which is not taken into account in the theory.

The simulation could be used in more detail to investigate the effects of friction on the system. Although it was shown that friction caused little effect to the condition over a small range of γs, the program could be run over many orders of magnitude of γ to prove this rigorously.

Alternatively, the model could be used to establish whether resonances can be manipulated to make the system jump from the lower to the upper stable point, and these results can be compared experimentally with the jigsaw.

As the equation of motion is analogous to the Mathieu equation, this project's results can be related to a wide range of physical systems with just a change of variables. Thus the observation that higher displacements from the vertical require larger stabilising frequencies has interesting implications in a number of fields, and potentially deserves further investigation.

References

[1] P. Machamer and B. Hepburn. Galileo and the pendulum: Latching on to time. In *The Pendulum: Scientific, Historical, Philosophical and Educational Perspectives*, pages 99–113. 2005.

[2] A. Stephenson. On induced stability. *Philosophical Magazine Series 6*, 15(86):233–236, 1908.

[3] P. L. Kapitza. Dynamic stability of the pendulum when the point of suspension is oscillating. *J. Exp. Theor. Phys.*, 21(5):588–597, 1951.

[4] P. L. Kapitza. Pendulum with vibrating axis of suspension. *Usp. Fizi. Nauk*, 44(1):7–20, 1954.

[5] M M Michaelis. Stroboscopic study of the inverted pendulum. *Am. J. Phys.*, 53(11):1079–1083, 1985.

[6] M M Michaelis and T Woodward. An inverted liquid demonstration. *American Journal of Physics*, 59(9):816–821, 1991.

[7] J A. Blackburn, H. J. T. Smith, and N Grønbech-Jensen. Stability and Hopf Bifurcations in an Inverted Pendulum. *American Journal of Physics*, 60(10):903–908, 1992.

[8] H P Kalmus. The inverted pendulum. *Am. J. Phys.*, 874:1–28, 1970.

[9] A. B. Pippard. The inverted pendulum. *Eur. J. Phys*, 203, 1987.

[10] E. Butikov. An improved criterion for Kapitza's pendulum stability. *Journal of Physics A: Mathematical and Theoretical*, 44(29):295202, 2011.

[11] L Ruby. Applications of the Mathieu equation. *American Journal of Physics*, 64(1):39, 1996.

[12] R Ramachandran and M Nosonovsky. Vibro-levitation and inverted pendulum: parametric resonance in vibrating droplets and soft materials. *Soft Matter*, 10(26):4633, 2014.

[13] W Paul. Electromagnetic Traps for Charged and Neutral Particles (Nobel Lecture). *Angewandte Chemie International Edition in English*, 29(7):739–748, 1990.

[14] N. P. Armitage. Cuprate superconductors:Dynamic stabilization? *Nature materials*, 13(JULY):665, 2014.

[15] E Butikov. On the dynamic stabilization of an inverted pendulum. *American Journal of Physics*, 69(7):755, 2001.

[16] E. Becker and G. K. Mikhailov. *Theoretical and Applied Mechanics*. Springer Science & Business Media, 1972.

[17] F. S. Crawford. Damping of a simple pendulum. *American Journal of Physics*, 43(3):276–277, 1975.

[18] D. Tong. *Lectures on Classical Dynamics*. University of Cambridge, 2015.

[19] F. M. Phelps and J. H. Hunter. An Analytical Solution of the Inverted Pendulum. *American Journal of Physics*, 33(1965):285, 1965.

[20] F. J. Vesely. *Computational Physics: An introduction*. Springer Science & Business Media, 2nd edition, 2012.

[21] J. Kiusalaas. *Numerical Methods in Engineering with Python*. Cambridge University Press, 2nd edition, 2010.

[22] H. J. T. Smith and J. A. Blackburn. Experimental study of an inverted pendulum. *Am. J. Phys*, 60(12):909–911, 1992.

[23] Harvard University. Harvard Natural Science Demonstrations.

[24] *Wickes PSJ800X Jigsaw Manual*. 2016.

[25] S. Timoshenko. *History of strength of materials*. McGraw-Hill New York, 1953.

[26] Elastic Properties and Young Modulus for some Materials, 2012.

[27] R. A. Serway. *Physics for Scientists and Engineers*. Saunders College Publishing, 2nd edition, 1986.

[28] TLP library DoITPoMS. Stiffness of long fibre composites, 2015.

[29] J. P. Davim. *Machinability of Fibre-Reinforced Plastics*. Walter de Gruyter GmbH & Co KG, 2015.

[30] PlumAmazing. PixelStick 2 Version 2.9, 2017.

[31] Health and Safety Executive UK. *Hand-arm vibration at work: A brief guide*. 2012.

A Appendix

A.1 Derivation of Lagrangian

The Lagrangian method allows us to describe the physical system in terms of the energies, rather than Newtonian time varying particle forces. We define the Lagrangian as:

$$L = T - V \tag{19}$$

where V is the gravitational potential energy and T is the sum of kinetic energies.

To find the moment of inertia consider a uniform rod with COM αl. The moment of inertia can be found from its definition:

$$\begin{aligned} I_{COM} = \int x^2 dm = \frac{M}{l}\int_{-\alpha l}^{(1-\alpha)l} x^2 dx \\ I_{COM} = \beta M l^2 = \frac{Ml^2}{3}(1 - 3\alpha + 3\alpha^2) \\ \beta(\alpha) = \frac{1}{3}(1 - 3\alpha + 3\alpha^2) \end{aligned} \tag{20}$$

The above definition can be used as we assume the radius of the rod is much shorter than the length l.

The total kinetic energy is found by considering the translational movement of the COM at velocity v_{COM}, and the energy of rotation about the COM:

$$T = \frac{1}{2}mv_{COM}^2 + \frac{1}{2}I_{COM}\dot{\theta}^2 \tag{21}$$

The linear velocity v_G^2 is found by considering time derivative of the co-ordinates, $\dot{x}$ and $\dot{y}$:

$$v_{COM}^2 = (\alpha l\dot{\theta})^2 + \dot{a}^2 + 2\dot{a}\alpha l\dot{\theta}\sin\theta \tag{22}$$

Thus we can fully describe the pendulum using the Lagrangian by combining (21) and (19):

$$\begin{aligned} L = \frac{1}{2}m\big[(\alpha l\dot{\theta})^2 + \dot{a}^2 + 2\dot{a}\alpha l\dot{\theta}\sin\theta\big] + \frac{1}{2}I_{COM}\dot{\theta}^2 \\ - mg(\alpha l\cos\theta + a(t)) \end{aligned}$$

A.2 Full derivation of Minimum Frequency

By writing θ as $\theta = \theta_1 + C\cos\Omega t + S\sin\Omega t$ and differentiating we find that:

$$\dot{\theta} = \dot{\theta}_1 + \dot{C}\cos\Omega t - \Omega C\sin\Omega t + \dot{S}\sin\Omega t + \Omega S\cos\Omega t$$

$$\begin{aligned} \ddot{\theta} = \ddot{\theta}_1 + \ddot{C}\cos\Omega t - 2\Omega\dot{C}\sin\Omega t - C\Omega^2\cos\Omega t \\ + \ddot{S}\sin\Omega t + 2\Omega\dot{S}\cos\Omega t - S\Omega^2\sin\Omega t \end{aligned}$$

Assuming C and S are small, we can use the angle formulas to write:

$$\sin\theta \approx \sin\theta_1 + \cos\theta_1(C\cos\Omega t + S\sin\Omega t)$$

To derive the equation of motion for θ_1 we will consider only the constant terms and the terms with frequency Ω. The constant terms give:

$$\ddot{\theta}_1 - f(\alpha)(\frac{g}{l}\sin\theta_1 + \frac{a\Omega^2}{2l^2}C\cos\theta_1) = 0$$

where $f(\alpha) = \frac{\alpha}{\alpha^2+\beta}$. Next consider the coefficients of $\cos\Omega t$ and $\sin\Omega t$:

$$\begin{aligned} -Cl^2\Omega^2 - f(\alpha)glC\cos\theta_1 = -f(\alpha)A\Omega^2 l\sin\theta_1 \\ -Sl^2\Omega^2 - glS\cos\theta_1 = 0 \end{aligned}$$

which are solved by $S = 0$ and

$$C = \frac{f(\alpha)A\Omega^2\sin\theta_1}{\Omega^2 l + f(\alpha)g\cos\theta_1}$$

As $\Omega^2 \gg g/l$, $C \approx f(\alpha)A\sin\theta_1/l$, and so can derive the equation of motion for θ_1:

$$\ddot{\theta}_1 + f(\alpha)(\frac{A^2\Omega^2 f(\alpha)}{2l^2} - \frac{g}{l})sin\theta_1 = 0$$

A.3 Friction

The friction is included in the equation of motion by using the dissipation function. If a force acts on a particle i in the x-direction, the power function is defined such that:

$$F_{i,x} = \frac{\delta P}{\delta\dot{x}_i} \tag{23}$$

By integrating (7), we can find the power function:

$$P = -\frac{K}{n+1} v^{(n+1)} \int sign(v)^{n+1} dv$$
$$= -\frac{K}{n+1} (\alpha l \dot{\theta})^{(n+1)} \int sign(\dot{\theta})^{n+1} d\dot{\theta} \quad (24)$$

where we have used $sign(v) = sign(\dot{\theta})$ Thus using these definitions can solve for F_θ and add it into the Lagrangian:

$$F_\theta = \frac{\delta P}{\delta \dot{\theta}} = -sign(\dot{\theta})^{n+1} K (\alpha l)^{n+1} (\dot{\theta})^n$$

In order to get equation into the same form of the SHM equation we can relabel the coefficient as γ as for this report we only consider the $\dot{\theta}$ dependence:

$$F_\theta = -sign(\dot{\theta})^{n+1} \gamma (\dot{\theta})^n$$

This means that when choosing γ we will be aware of varying orders of magnitude depending on n.

A.4 Full derivation of RKF Method

The RKF method is embedded, where two approximations for the solution are made at each step, one of order 4 and one of order 5. Depending on the agreement of the two answers, h is accepted, increased or decreased.

This is beneficial computationally as one extra calculation allows the algorithm to adapt the step size h to a specified accuracy, thus removing the issue of guessing the optimal value of h. Each step requires 6 calculations:

$$\mathbf{K}_0 = h\mathbf{F}(x, y)$$
$$\mathbf{K}_i = h\mathbf{F}(x + A_i h, y + \sum_{j=0}^{i-1} B_{ij}\mathbf{K}_j), \quad i = 1, 2, ..., 5 \quad (25)$$

The approximations of the next step are found using the values for $\mathbf{K}_i$. For the fourth order formula($\mathbf{y}_4$) and fifth order formula($\mathbf{y}_5$):

$$\mathbf{y}_5(x + h) = \mathbf{y}(x) + \sum_{i=0}^{5} C_i \mathbf{K}_i \quad (26)$$

$$\mathbf{y}_4(x + h) = \mathbf{y}(x) + \sum_{i=0}^{5} D_i \mathbf{K}_i \quad (27)$$

The coefficients (A_i, B_{ij}, C_i, and D_i) are the Cash-Karp coefficients and are summarised in the Butcher tableau.[21]

The solution is advanced by $\mathbf{y}_5$ whilst $\mathbf{y}_4$ is used to estimate the truncation error. This is the error of estimating an infinite sum as a finite sum, which goes as $O(h^n)$ for a nth order RK method.

The magnitude of the per step error, $e(h)$, is taken as the root-mean-square difference between the two formulas, $\mathbf{E}(h) = \mathbf{y}_5 - \mathbf{y}_4$:

$$e(h) = \tilde{E}(h) = \sqrt{\frac{1}{n} \sum_{i=0}^{n-1} E_i^2(h)} \quad (28)$$

with this solution cheap computationally as the two formulas evaluate the function at the same points.

The truncation error arises from the root-mean-square difference between the two formulas, $\mathbf{E}(h) = \mathbf{y}_5 - \mathbf{y}_4$.

This estimated local error, e, is then used to adjust the step-size so that the error is approximately equal to required tolerance ϵ. As the truncation error for fourth order goes as $O(h^5)$, if we perform a step h_1 with error e_1, we can calculate the optimal step-size h_2 that gives an error equal to ϵ:

$$h_2 = 0.9 h_1 \Big(\frac{e(h_1)}{\epsilon} \Big)^{\frac{1}{5}} \quad (29)$$

The extra 0.9 is added as a small margin of safety due to the approximation earlier. If $h_2 \geq h_1$, then h_1 is accepted, otherwise the integration is repeated with h_2.

Additionally as $e(h)$ is a very conservative estimate for the actual error, the overall tolerance is the same as each local tolerance. For large numbers of steps, this becomes no longer valid

and so ϵ_{local} will be decreased accordingly.

A.5 Error Calculation

When calculating errors in this project, we will consistently use the Taylor expansion method. If we have some function $f(x, y, z)$ the error in f to first order will be calculated using:

$$\sigma_f^2 = \left(\frac{\delta f}{\delta x}\right)^2 \sigma_x^2 + \left(\frac{\delta f}{\delta y}\right)^2 \sigma_y^2 + \left(\frac{\delta f}{\delta z}\right)^2 \sigma_z^2 \quad (30)$$

We can use this general formula to derive simpler forms for specific circumstances, namely $f = x + y$ and $f = \frac{x}{y}$.

For $f = x + y$, (30) becomes:

$$\sigma_f^2 = \sigma_x^2 + \sigma_y^2 \quad (31)$$

and for $f = \frac{x}{y}$:

$$\left(\frac{\sigma f}{f}\right)^2 = \left(\frac{\sigma_x}{x}\right)^2 + \left(\frac{\sigma_y}{y}\right)^2 \quad (32)$$

Error in γ is found from:

$$\sigma_\gamma^2 = \left(\frac{\delta \gamma}{\delta X}\right)^2 \sigma_\gamma^2 \quad (33)$$

where $X = ln(\frac{\theta_{max}}{\theta_0})$. The error σ_t is neglected as $\sigma_t << \sigma_X$

The error of X is also needed. Using the properties of logs, it is easy to show that:

$$\sigma_x = \sqrt{2}(\frac{\theta_0}{\theta_{max}})\sigma_{\theta_0} \quad (34)$$

with an extra factor of $\sqrt{2}$ arising from the fact $\sigma_{\theta_0} = \sigma_{\theta_{max}}$

Error in angular frequency is found from multiplying the percentage error in the period by Ω as the relationship is the same as f(x)=1/x.

$$\sigma_x = \sqrt{2}(\frac{\theta_0}{\theta_{max}})\sigma_{\theta_0} \quad (35)$$

Error in Ω found by using the taylor expansion for variables α, A, and l.

$$\sigma_\Omega^2 = \left(\frac{\delta \Omega}{\delta \alpha}\right)^2 \sigma_\alpha^2 + \left(\frac{\delta \Omega}{\delta l}\right)^2 \sigma_l^2 + \left(\frac{\delta \Omega}{\delta A}\right)^2 \sigma_A^2 \quad (36)$$

The main source of error is in the amplitude A so we can approximate the equation to just the term proportional to A.

A.6 n=0

The $n = 0$ friction term was inputted into our model and compared to the data, but the constant friction caused a more linear decay as shown in figure 23. This meant that there were no oscillations at smaller angles and so $n = 0$ was immediately discarded as a solution.

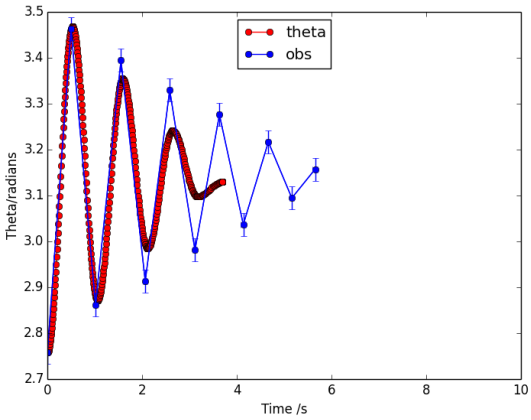

Figure 23: Comparison of the data to $n = 0$ model with $\theta_0 = 2.7^c$. There is a linear decay and no oscillations at small angles. Error bars are $\pm 0.025^c$

A.7 Tolerance change

In order to see behaviour for $t > 20secs$ the tolerance had to be decreased to reach this maximum time, due to the larger truncation error accumulation. The behaviour of the step just below the threshold Ω is shown in figure 19 and the behaviour closely matches the θ behaviour from above, with a decrease in h due to an increase in θ.

Lowering the tolerance too much (i.e. to 10^{-5}) decreases the resolution of the numerical integration, and the minimum Ω_c becomes $0.5rads^{-1}$ larger. Thus a compromise had to be taken between accuracy and length of motion and a tolerance of 10^{-6} was used for dynamics over twenty seconds long.

A.8 Linear regression to find γ

Below are the linear regressions for $l = 100 - 400mm$ for the two different regimes, $5° \leq \phi \leq 20°$ and $0° \leq \phi \leq 5°$.

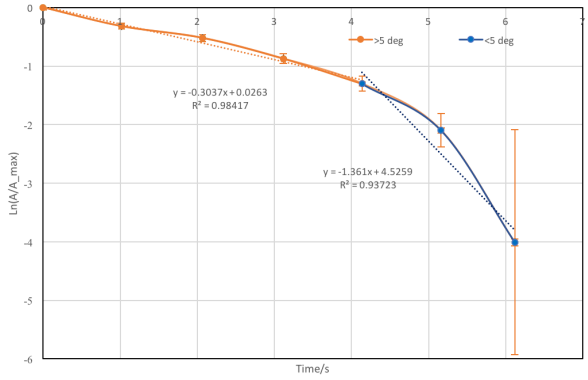

Figure 24: Detailed plot of logarithmic behaviour for $L = 427mm$. Linear regression was performed for $5° \leq \phi \leq 20°$ and $0° \leq \phi \leq 5°$ regimes.

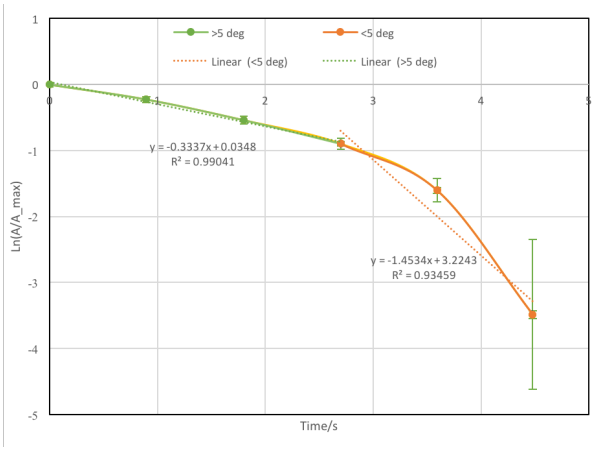

Figure 25: Detailed plot of logarithmic behaviour for $L = 327mm$. Linear regression was performed for $5° \leq \phi \leq 20°$ and $0° \leq \phi \leq 5°$ regimes.

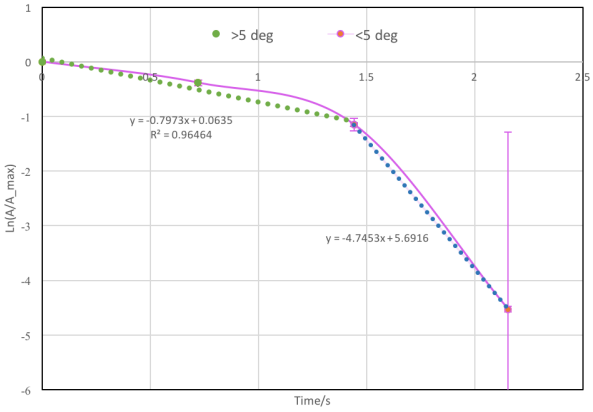

Figure 26: Detailed plot of logarithmic behaviour for $L = 227mm$. Linear regression was performed for $5° \leq \phi \leq 20°$ and $0° \leq \phi \leq 5°$ regimes.

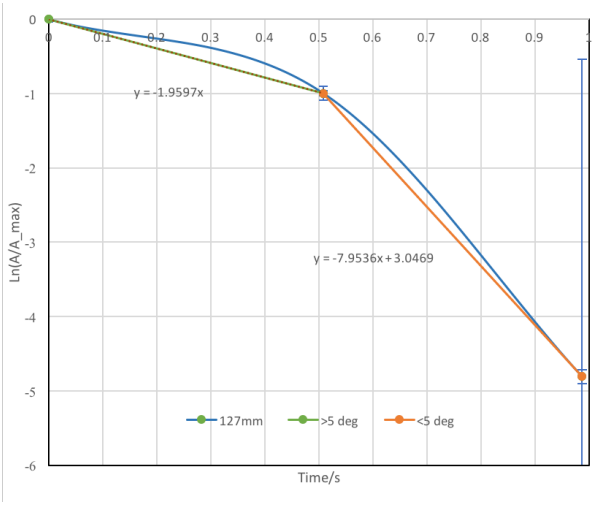

Figure 27: Detailed plot of logarithmic behaviour for $L = 127mm$. Linear regression was performed for $5° \leq \phi \leq 2°0$ and $0° \leq \phi \leq 5°$ regimes.